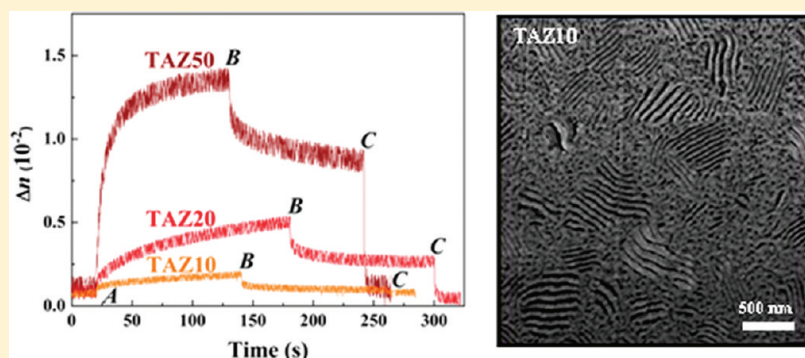


Reversible Optical Storage Properties of Nanostructured Epoxy-Based Thermosets Modified with Azobenzene Units

Raquel Fernández, Jose Angel Ramos, Leandro Espósito, Agnieszka Tercjak, and Iñaki Mondragon*

Materials + Technologies Group, Department of Chemical & Environmental Engineering, Polytechnic School, Universidad del País Vasco/Euskal Herriko Unibertsitatea, Pza Europa 1, 20018 Donostia-San Sebastián, Spain

ABSTRACT:



Azo-containing polymers are of particular interest in the design of materials for applications in optical recording. The aim of this contribution was the synthesis and characterization of optically active epoxy-based nanostructured thermosets obtained using epoxidized poly(styrene-*b*-butadiene-*b*-styrene) (SBS) as templating agent and modified with azobenzene groups. Morphological analysis by means of atomic force microscopy, as well as an investigation about the anisotropic optical properties of the developed materials was carried out. Different types of morphologies from micelles without long-range order to nanostructures with long-range order were achieved depending on the content of epoxidized block copolymer and azobenzene, and on the extent of epoxidation of butadiene blocks. In addition, the study of optical anisotropy showed a clear dependence of the optical storage properties upon the concentration of azo-chromophore in the samples. In particular, a thermoset containing 12.3 wt % of azo-dye and 5 phr of SBS with 46 mol % of butadiene blocks epoxidized revealed a spherical micellar morphology with maximum birefringence in the order of 1.8×10^{-2} and residual fraction of birefringence of around 0.3 after several weeks of turning *off* the writing beam. Besides, numerous writing-erasing cycles could also be performed without photodegradation of the materials. Furthermore, comparing parent thermosets and nanostructured systems, similar birefringence values were obtained with the advantage that the latter can also be used as templates for the development of multifunctional advanced thermosetting materials with optical properties.

INTRODUCTION

Over the last years, photonics has emerged as a major interdisciplinary field of science and technology with a focus on the transport and manipulation of light. Rapid progress in photonics has been achieved because of continuous advances in nanotechnology, materials science, optics, physics, among other areas.¹

Polymers play an important role in the development of materials for photonics. They are relatively inexpensive materials that can be functionalized to achieve required properties, they themselves can possess useful optical properties like photoluminescence, and they can also act as matrices for optically active species such as inorganic nanoparticles, quantum dots, liquid crystals, or dyes.^{1–6} Notably, azobenzene serves as the parent molecule to a wide range of dyes and nonlinear optical chromophores. In addition, changes that can be imparted to polymers when azobenzene is part of their structures or is associated with them can help to develop new applications in the field. Indeed, reversible photoisomerization in azo-containing polymers

enables the use of light as a powerful external stimulus to control or trigger the change of the properties of these materials. For this reason, there has been considerable worldwide research devoted to azo-polymers, ranging from fundamental studies to exploitation for applications. Most research has dealt with the physical and optical properties of azo-polymers interesting for applications in the area of reversible optical storage.^{7–13}

Epoxy resins represent a family of thermosetting polymers known from many decades ago. The wide diffusion they have found on the market is a consequence of their extreme versatility and their excellent attributes, such as abrasion resistance, thermal stability, chemical resistance and mechanical properties. Those features make them primary candidates for a wide range of applications among which epoxy thermosets stand out as high performance matrices in advanced composites, coatings, adhesives, and laminates.

Received: August 8, 2011

Revised: October 14, 2011

Published: November 22, 2011

Thus, researchers have focused mainly on the study of their mechanical and thermal properties.^{14–16} However, epoxy networks are also transparent and, therefore, suitable for optical applications, even though these have not been explored so much as the mechanical ones.

On this basis and taking into account the need for new materials with specific functionalities appropriate for emerging technological applications, preparation of thermosets based on epoxy resins for optical applications can be of interest. In addition, nanostructured thermosets are a relatively new class of advanced materials which are able to improve the mechanical properties of conventional thermosetting polymers retaining their optical transparency.^{17–19} In fact, block copolymers (BCP), owing to their capability to form nano-scale structures, are widely used as templates for generating nanostructured epoxy matrices with long-range order.^{20–23} One way to achieve this goal is through reaction-induced microphase separation (RIMS) of one of the blocks during curing, both being initially miscible with the epoxy resin. In the case of BCP with both blocks immiscible with the epoxy system after curing, one feasible approach to promote the compatibilisation of one of the blocks with the epoxy matrix can be its chemical modification. For instance, poly(styrene-*b*-butadiene-*b*-styrene) (SBS) block copolymers can be randomly epoxidized with this objective. This methodology has been satisfactorily employed in our group to generate stable nanostructures in epoxy matrices.^{24,25} Additionally, nanostructured thermosetting systems can also act as a template for the incorporation of inorganic nanoparticles with particular properties with the aim of developing multifunctional materials, which is the current challenge of many researchers.²⁶

The present work is oriented toward the development of novel nanostructured epoxy systems containing azobenzene groups for reversible optical storage. With this goal in mind, azo-containing epoxy/amine formulations were modified with epoxidized SBS to promote the compatibilisation of the polybutadiene (PB) block with the epoxy matrix. On this way nanostructured epoxy thermosets containing azobenzene groups have been achieved, due to reaction-induced microphase separation of polystyrene (PS) block. Optical and morphological properties of the resulting nanostructured materials were evaluated and discussed considering several variables as epoxidation extent, epoxidized SBS content, and azobenzene concentration in the epoxy matrix.

EXPERIMENTAL SECTION

Synthesis of Azo-Containing Nanostructured Epoxy Thermosets. *Materials.* Amphiphilic linear SBS block copolymer, C540, with 40 wt % PS was kindly supplied by Repsol-YPF. A push–pull azo-dye, 4-(4-nitrophenylazo)aniline ($\text{O}_2\text{N}(\text{C}_6\text{H}_4)\text{N}=\text{N}(\text{C}_6\text{H}_4)(\text{NH}_2)$), Disperse Orange 3 (DO3), with a melting temperature of 200 °C, was purchased from Aldrich. An epoxy resin, diglycidyl ether of bisphenol A (DGEBA), DER 332 $n = 0.03$, with an epoxy equivalent of 175 g equiv^{−1}, was kindly provided by Dow Chemical. As hardener, we employed an aromatic diamine, 4,4'-methylene-bis(3-chloro-2,6-diethylaniline) (MCDEA), supplied by Lonza. All materials were used as received without further purification.

Different randomly epoxidized SBS block copolymers, SBSe_p_x (x being the extent of epoxidation, mol %, with respect to PB double bonds determined by ¹H NMR), were obtained by epoxidation of PB blocks. This reaction was carried out using hydrogen peroxide in the presence of an *in situ* prepared catalyst system in a water/dichloroethane biphasic mixture, following a procedure described elsewhere.²⁴

Curing Protocol. A thermoplastic azo-prepolymer (TAZ) was synthesized by reaction between DO3 and DGEBA following a procedure

previously described.²⁷ It was prepared in a stoichiometric ratio $r = \text{DO3 equiv/DGEBA equiv} = 0.5$ to achieve reaction products with epoxy groups in the extreme of chains. Then, TAZ was blended in different ratios (10, 20, or 50 wt %) with DGEBA, MCDEA, and various amounts of SBSe_p_x (from 5 to 50 phr) to prepare different azo-containing epoxy systems. Dichloroethane was used as solvent to obtain homogeneous samples. Before curing the solvent was removed by evaporation at room temperature. All samples were then cured at 140 °C during 24 h and postcured at 165 °C for 2 h. An amino-hydrogen-to-epoxy stoichiometric ratio equal to 1 was maintained for all prepared systems. A brief description of all samples studied is presented in Table 1. Epoxy thermosets without BCP were named according to their content in thermoplastic azo-prepolymer as TAZ_y (y being TAZ ratio (wt %)). Nanostructured systems were named according to their content both in TAZ and epoxidized SBS as TAZ_y–SBSe_p_x_z (z being the SBSe_p_x ratio (phr)).

Characterization of Azo-Containing Nanostructured Epoxy Thermosets. *Differential Scanning Calorimetry Measurements.* Differential scanning calorimetry (DSC) was performed using a Mettler Toledo DSC 192 822 differential scanning calorimeter equipped with a sample robot 193 TSO 801 RO. Nitrogen was used as purge gas (10 mL min^{−1}). The glass transition temperature (T_g), defined as the onset of the change in specific heat, was determined from the thermograms obtained in heating scans at 10 °C min^{−1}.

Morphological Analysis. For the morphological study the reactive solutions were drop cast into polytetrafluoroethylene molds of 4 cm × 4 cm × 1 cm. After that, the solvent was removed and the curing schedule described above was performed. Samples of cured mixtures were prepared using an ultramicrotome (Leica Ultracut R) equipped with a diamond knife.

The morphology of the samples was studied by atomic force microscopy (AFM). AFM images were obtained with a Nanoscope IIIa scanning probe microscope (Multimode, Digital Instruments). Tapping mode (TM) in air was employed using an integrated tip/cantilever (125 μm in length with *ca.* 300 kHz resonant frequency and spring constant of *ca.* 40 N/m). Typical scan rates during recording were 0.7–1 line s^{−1} using a scan head with a maximum range of 16 μm × 16 μm.

Optical Analysis. For the analysis of optical properties films of all nanostructured systems were prepared onto clean glass slides by spin-coating from 5 wt % reactive solutions in dichloroethane, using a P6700 spin-coater from Cookson Electronics. The spinner program was 1000 rpm for 30 s and 2000 rpm for 30 s or 200 rpm for 60 s and 1000 rpm for 30 s, depending on the required thickness. Residual solvent was removed by evaporation at room temperature and, then, samples were cured following the experimental conditions mentioned above. Film thicknesses were calculated from topographic AFM images of scratched films, taking into account the difference in height between a flat area of the sample and the surface of the clean glass slide. Relatively homogeneous thin films of variable thicknesses between 500 ± 50 nm and 1000 ± 100 nm were obtained.

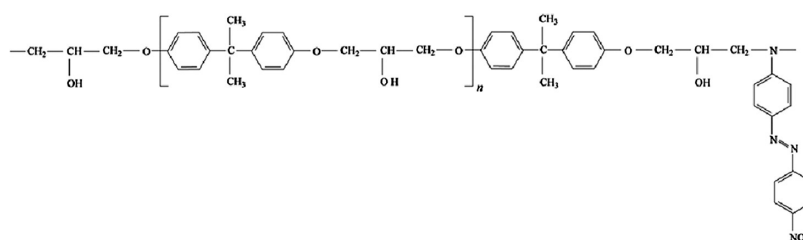
Optical storage experiments were carried out at room temperature and under ambient conditions. The experimental setup used was similar to that previously reported.²⁷ Optical birefringence was induced in films of the obtained azo-containing materials using a linearly polarized argon laser operating at 488 nm (writing beam) with a polarization angle of 45° with respect to the polarization direction of a low power He–Ne laser operating at 632.8 nm (reading beam). The power of the writing beam used in the experiments was varied between 4 and 24 mW on a spot of 0.4 mm² and the change in the transmission of the reading beam, which passed through the sample between two crossed polarizers, was measured with a photodiode. The induced birefringence (Δn) was determined by measuring the reading beam transmission ($T = I/I_0$) according to

$$\Delta n = (\lambda/\pi d) \sin^{-1}(I/I_0)^{1/2}$$

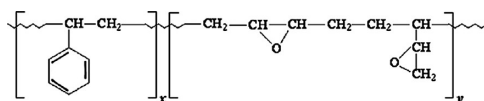
Table 1. Description of the Samples Used

sample code	TAZ ^a (wt %)	DGEBA/MCDEA (wt %)	SBSep ^b (phr ^c)
TAZ10	10	90	0
TAZ10-SBSep ₃₇ 10	10	90	10
TAZ10-SBSep ₃₇ 30	10	90	30
TAZ10-SBSep ₃₇ 50	10	90	50
TAZ10-SBSep ₄₆ 50	10	90	50
TAZ20	20	80	0
TAZ20-SBSep ₃₇ 10	20	80	10
TAZ20-SBSep ₃₇ 20	20	80	20
TAZ20-SBSep ₃₇ 30	20	80	30
TAZ20-SBSep ₄₆ 20	20	80	20
TAZ50	50	50	0
TAZ50-SBSep ₃₇ 5	50	50	5
TAZ50-SBSep ₃₇ 10	50	50	10
TAZ50-SBSep ₃₇ 30	50	50	30
TAZ50-SBSep ₄₆ 5	50	50	5

^a Defined as thermoplastic azo-prepolymer.



^b Defined as randomly epoxidized poly(styrene-*b*-butadiene-*b*-styrene).



^c Defined as per hundred resin.

where λ is the wavelength of the reading beam, d is the film thickness, I is the intensity of the reading beam after the second polarizer and I_0 is the transmitted intensity of the reading beam between parallel polarizers in absence of anisotropy.

Previous to optical experiments films were heated above T_g of the epoxy thermosets and subsequently stored at room temperature. In addition, each photo-orientation experiment was done on a different previously nonirradiated spot so as to avoid irradiation history complications.

RESULTS AND DISCUSSION

Morphological Analysis. Nanostructured epoxy systems containing an azo-dye were achieved by modification with epoxidized SBS block copolymer. Specifically, azobenzene groups were introduced via chemical bonding between TAZ and DGEBA/MCDEA system, the thermoplastic azo-prepolymer being therefore part of the epoxy matrix. All the epoxy-based networks studied had the azo-chromophore placed in a branch, also called cross-linked side chain.¹²

The morphologies generated were investigated using TM-AFM. In particular, the effects of azobenzene content, epoxidized SBS ratio and epoxidation extent of butadiene blocks on nanostructuring were analyzed. As shown in our previous work,²⁸

random epoxidation of PB block at high extent leads to miscibility of this block with the epoxy matrix and segregation of PS block during network formation, thus achieving long-range order nanostructures. It should be noted that in this work TAZ was part of the epoxy network, which withdrew PS chains during curing. As published by Ocando et al.,²⁵ it has to be taken into account that two different mechanisms can be involved through morphology development during curing as a function of epoxidized PB content in DGEBA/MCDEA systems modified with epoxidized SB block copolymers. On the one hand, reaction-induced microphase separation of PS block leads to long-range order nanostructures and, on the other hand, combination of both self-assembly of epoxidized PB block in the initial mixture and RIMS of PS block can give rise to vesicles or long worm-like micelles with a bilayered structure.²⁵ In this work, additionally, we found that the presence of the thermoplastic azo-prepolymer provoked a decrease of miscibility of initial mixtures before curing, leading to different morphologies as a function of TAZ content owing to the modification of interactions between groups with respect to the modified matrices without TAZ, as discussed below.

Figure 1 shows TM-AFM phase images of cured epoxy systems modified with different amounts of SBSep₃₇ (10 and 30 phr) containing several TAZ ratios (10, 20, and 50 wt %).

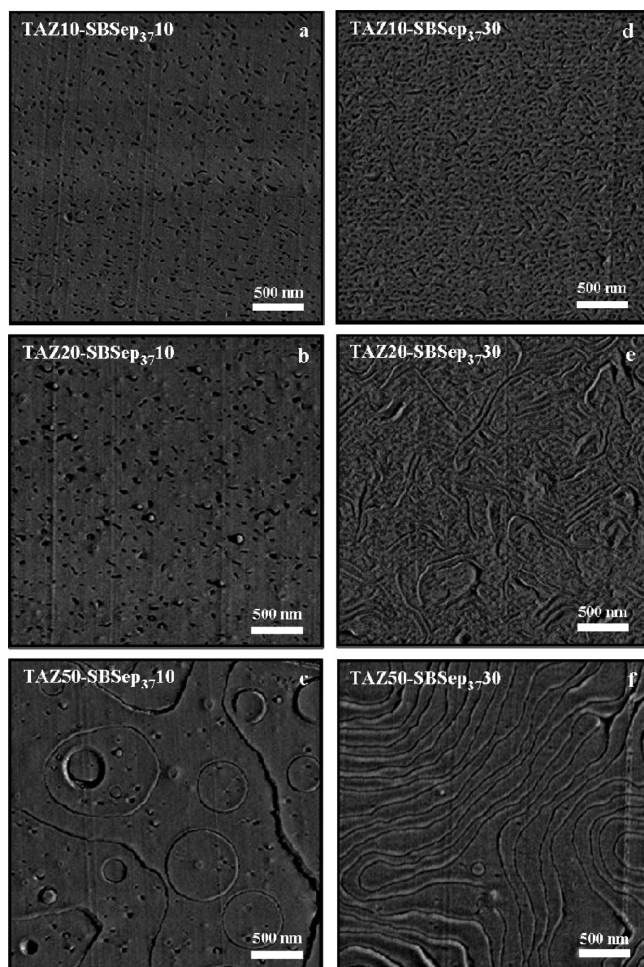


Figure 1. TM-AFM phase images of epoxy thermosets modified with 10 phr SBSep₃₇ containing (a) 10 wt % TAZ, (b) 20 wt % TAZ, and (c) 50 wt % TAZ and epoxy thermosets modified with 30 phr SBSep₃₇ containing (d) 10 wt % TAZ, (e) 20 wt % TAZ, and (f) 50 wt % TAZ ($3 \mu\text{m} \times 3 \mu\text{m}$).

This epoxidation extent (37 mol %) was above the miscibility threshold with the epoxy resin, which is set to 27 mol % using MCDEA as hardener.²⁸ Only phase images are shown due to the resemblance of height and phase TM-AFM images of each sample. As can be observed, in all cases microphase separation was achieved. TAZ10-SBSep₃₇10 cured epoxy system showed micellar nanodomains of PS block in the epoxy matrix. The size of these microphase-separated domains was around 30 nm in diameter. Increasing of the thermoplastic azo-prepolymer content to 20 wt % (TAZ20-SBSep₃₇10) led to higher amount of segregated domains. For TAZ50-SBSep₃₇10 cured system co-existence of nanodomains with around 30 nm in diameter, interconnected long worm-like micelles and spherical structures with diameters ranging from around 70 to 1000 nm was achieved. These morphological variations were probably related to the fact that increasing TAZ content, the miscibility between the block copolymer and the epoxy system before curing decreased. Here it should be pointed out that PS homopolymer is miscible with DGEBA/MCDEA system at temperatures higher than 90 °C.²⁵ On the other side, increasing of the PB epoxidation extent and the ratio between pure epoxy resin and TAZ led to higher compatibility between the block copolymer and the epoxy

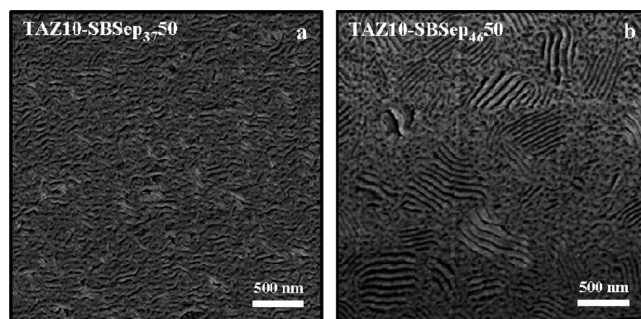


Figure 2. TM-AFM phase images of epoxy thermosets containing 10 wt % TAZ and modified with 50 phr: (a) SBSep₃₇ and (b) SBSep₄₆ ($3 \mu\text{m} \times 3 \mu\text{m}$).

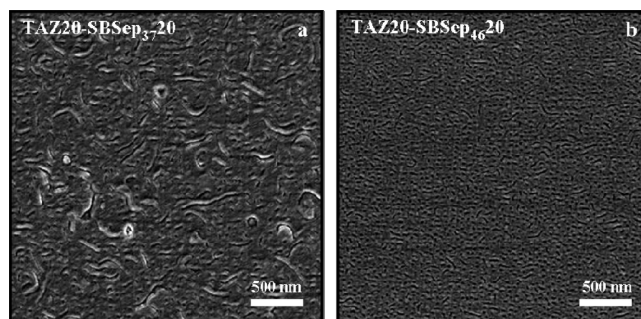


Figure 3. TM-AFM phase images of epoxy thermosets containing 20 wt % TAZ and modified with 20 phr: (a) SBSep₃₇ and (b) SBSep₄₆ ($3 \mu\text{m} \times 3 \mu\text{m}$).

matrix. Therefore, taking into account the initial miscibility of blocks with the epoxy system before curing, for 37 mol % of epoxidation extent one can expect the formation of segregated structures in the epoxy matrix through self-assembly of epoxidized PB occurred prior to curing, followed by fixing these structures through reaction-induced microphase separation of PS chains during network formation. Results confirmed that for investigated systems this process was favored by the increase of TAZ content. Thus, various morphologies, through combination of self-assembly of PB block and RIMS of PS block, were generated as consequence of variations in interactions between groups in the initial mixtures.

In addition, increase of PS content with increasing SBSep₃₇ content from 10 to 30 phr led to longer segregated structures. As reported by Ocando et al.,²⁸ for enough PB epoxidation, the morphologies generated in the same kind of thermosetting systems without azo-dye depend strongly on PS content in the initial mixture. On the other side, it is worth to note that larger segregated structures were achieved for thermosetting systems with 30 phr SBSep₃₇ as increasing TAZ content, due to a decrease of miscibility between the epoxy-precursor mixture and the block copolymer that led to self-assembled segregation of some amount of PB block before curing.

Furthermore, as shown in Figures 2–4, increase of the epoxidation extent provoked higher miscibility between epoxidized PB block and epoxy matrix and, consequently, long-range order nanostructures were achieved. Indeed, when increasing the epoxidation extent from 37 up to 46 mol % (Figure 2), the system containing 10 wt % TAZ and 50 phr BCP revealed PS cylinders

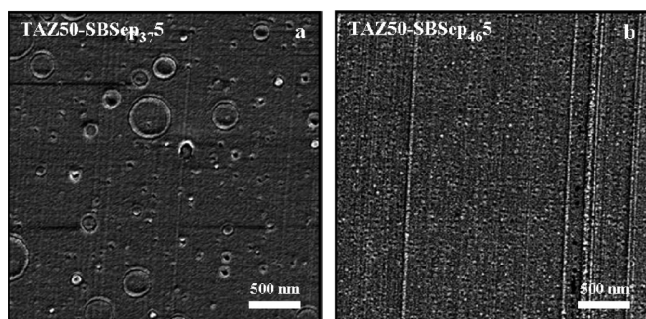


Figure 4. TM-AFM phase images of epoxy thermosets containing 50 wt % TAZ and modified with 5 phr: (a) SBSeP₃₇ and (b) SBSeP₄₆ (3 $\mu\text{m} \times 3 \mu\text{m}$).

inside the matrix mixture. The thermosetting system containing 20 wt % TAZ and 20 phr BCP showed worm-like structures (Figure 3), while for the system containing 50 wt % TAZ and 5 phr BCP spherical micellar nanostructures with around 30 nm in diameter were achieved (Figure 4) with the same increase in the epoxidation extent. Thus, in general, as decreasing the epoxidation extent, structures with a less curved interface with the epoxy system than with higher epoxidation extent were formed, therefore leading to spherical and cylindrical micelles.

According to previous work done in our group,²⁵ as well as by other authors, such as Dean et al.²¹ who established that for low contents of block copolymer phase transitions from spherical micelles to worm-like micelles and, finally, to vesicles took place as the volume fraction of immiscible block increased, results presented here suggest that 46 mol % of epoxidation extent was needed to achieve long-range order nanostructuring because of the higher compatibility of the more epoxidized SBS with the epoxy-precursor mixture. Consequently, for 46 mol % of epoxidation extent morphologies were originated through reaction-induced microphase separation of PS block starting from a miscible mixture before curing. On the contrary, 37 mol % of epoxidation extent was not enough to make compatible all not randomly epoxidized PB chains with the epoxy-precursor mixture before curing. Thus, morphologies were developed through self-assembly before curing followed by fixing the nanostructures via phase separation of PS chains through curing reaction, leading to different segregated structures depending on the content of block copolymer and thermoplastic azo-prepolymer. Furthermore, miscibilisation of initial mixtures was favored not only as increasing the epoxidation extent, but also as decreasing TAZ content, since a significant amount of randomly epoxidized PB chains could not be miscibilised before curing when high quantities of TAZ were incorporated into the epoxy system.

Analyzing together Figures 1–4 and focusing on SBSeP₃₇ content, for the lowest azobenzene ratio (10 wt % TAZ) the morphology evolved from micelles with around 30 nm in diameter for 10 phr SBSeP₃₇ (Figure 1a) to worm-like nanostructures without long-range order for 50 phr SBSeP₃₇ (Figure 2a). For the sample with 20 wt % TAZ longer microphase-separated structures were achieved when increasing SBSeP₃₇ content from 10 to 30 phr (Figures 1b, 3a, and 1e). Finally, for the highest azobenzene content (50 wt % TAZ), various morphologies were achieved as a function of SBSeP₃₇ ratio. TAZ50-SBSeP₃₇5 cured epoxy system (Figure 4a) showed a combination of separated nanodomains with around 30 nm in diameter and spherical structures. For TAZ50-SBSeP₃₇10

Table 2. Birefringence Values and Glass Transition Temperatures of the Samples Used

sample code	DO3 (wt %)	T_g (°C)	Δn (10^{-2})	Δn_N (10^{-2})
TAZ10	2.58	155	0.33 ± 0.08	0.13
TAZ10-SBSeP ₃₇ 10	2.35	142	0.27 ± 0.03	0.11
TAZ10-SBSeP ₃₇ 30	1.98	121	0.24 ± 0.04	0.12
TAZ10-SBSeP ₃₇ 50	1.72	83	0.21 ± 0.01	0.12
TAZ10-SBSeP ₄₆ 50	1.72	79	0.20 ± 0.04	0.11
TAZ20	5.16	153	0.85 ± 0.14	0.16
TAZ20-SBSeP ₃₇ 10	4.69	141	0.81 ± 0.12	0.17
TAZ20-SBSeP ₃₇ 20	4.30	134	0.64 ± 0.09	0.15
TAZ20-SBSeP ₃₇ 30	3.97	122	0.55 ± 0.13	0.14
TAZ20-SBSeP ₄₆ 20	4.30	130	0.64 ± 0.01	0.15
TAZ50	12.9	139	1.90 ± 0.12	0.15
TAZ50-SBSeP ₃₇ 5	12.3	138	1.70 ± 0.08	0.14
TAZ50-SBSeP ₃₇ 10	11.7	134	1.70 ± 0.12	0.15
TAZ50-SBSeP ₃₇ 30	9.92	121	1.45 ± 0.32	0.15
TAZ50-SBSeP ₄₆ 5	12.3	138	1.80 ± 0.11	0.15

(Figure 1c) in addition interconnected long worm-like micelles appeared and for TAZ50-SBSeP₃₇30 (Figure 1f), as the ratio of segregated block copolymer increased, the morphology evolved to a geometry with less interfacial curvature.

Optical Analysis. In relation to the optical storage abilities of azo-containing materials, the information is stored in the form of photoinduced anisotropy in this kind of systems.²⁹ Optical anisotropy is a birefringence optically induced in polymeric films as a result of a reorientation of the azo-chromophores via a statistical selection process. Normally, linearly polarized light is employed to provoke a *trans*–*cis* isomerization followed by a molecular reorientation and a *cis*–*trans* isomerization. The absorption and reorientation sequence will be repeated until the azobenzene molecules dipole moment lies in a direction which is perpendicular to the polarization direction of the writing beam. Working on the principle that some of the fundamental attributes a material requires to be employed as an optical memory media are high storage capacity, fast response, stability during writing-erasing cycles and long-term stability. The parameters we wanted to investigate were the maximum level of achievable birefringence and the rate of birefringence growth, as well as the thermal relaxation rate and the long-term stability of the induced birefringence. In addition, there are a series of aspects affecting those variables, including chemical factors (such as type of azo-chromophore, azobenzene content, T_g , structure of the polymeric main chain, ...) and physical ones (such as irradiation wavelength and intensity, film thickness, history of the sample, operating temperature, ...).^{10,13,30–34} All of them were taken into consideration in the present work.

First, the maximum anisotropy that can be photoinduced in the samples was evaluated. Table 2 shows the birefringence values and glass transition temperatures of all prepared epoxy systems. Since birefringence depends on the azobenzene quantity, Δn_N values, the birefringence data normalized to the azo-dye content (Δn divided by wt % DO3), have also been reported. As can be seen, Δn data varied from 0.2×10^{-2} to 1.9×10^{-2} as the azo-chromophore increased from 1.72 to 12.9 wt %. These birefringence values can be considered adequate for optical applications taking into account the low azobenzene concentrations used and the reported values for this kind of materials.^{35–37}

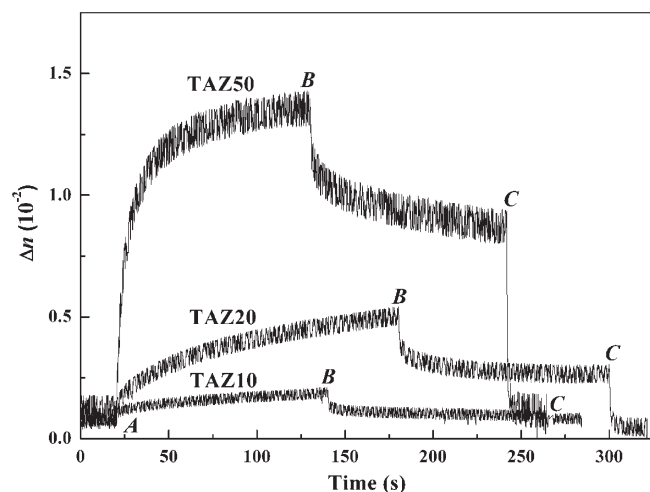


Figure 5. Typical writing, relaxing, and erasing curves for systems containing 30 phr SBSep₃₇. The power of the writing beam is 6 mW.

Nevertheless, it should be noted that no significant differences in Δn_N could be seen between parent azo-containing thermosets and the ones modified with epoxidized SBS. Therefore, nanostructuring did not have a significant influence on the maximum level of achievable birefringence, which means the interactions among azobenzene groups were similar in both kind of systems, because in all cases they were covalently linked to the epoxy network via chemical bonding between TAZ and DGEBA/MCDEA system. However, a slight increase in Δn_N was perceptible when increasing TAZ content, probably due to an increase of interactions between azobenzene units, as a consequence of the increase in azo-dye concentration.

The formation, relaxation and erasing of birefringence is illustrated in a more descriptive way in Figure 5 by writing-relaxing-erasing sequences obtained for the systems TAZ10, TAZ20, and TAZ50 with 30 phr SBSep₃₇. Initially there was no transmission of the reading beam, which continuously illuminated the samples, since azobenzene molecules in *trans* form were randomly distributed. At point A, the writing beam was turned *on* and the reading beam was transmitted through the crossed polarizers due to the optical anisotropy induced in the films as a consequence of *trans*–*cis*–*trans* photoisomerisations that led to the orientation of *trans* molecules perpendicular to the polarization vector of the writing beam. In consequence, birefringence was rapidly built up to the saturation level. Indeed, the optical anisotropy level increased as the azobenzene content was higher ($\Delta n = 0.24 \times 10^{-2}$ for TAZ10, $\Delta n = 0.55 \times 10^{-2}$ for TAZ20, and $\Delta n = 1.45 \times 10^{-2}$ for TAZ50) since Δn is the result of photoinduced orientation of the azo-chromophores. Hence, larger number of photoactive units in the polymer chains generated a higher birefringence. This photoinduced anisotropy represents a writing mechanism in an optical storage device. When the writing beam was turned *off* at point B, Δn rapidly fell *off* initially, due to thermally activated dipole reorientation which would tend toward randomization of the anisotropy. Thereafter, Δn became stable in a relaxed level, where the rate of change of anisotropy was very small. This fact proved that the birefringence was not completely preserved after writing with linear polarized light, even though a significant amount of optically induced orientation was conserved. The stable birefringence pattern or remaining birefringence corresponds to the storage step. Finally,

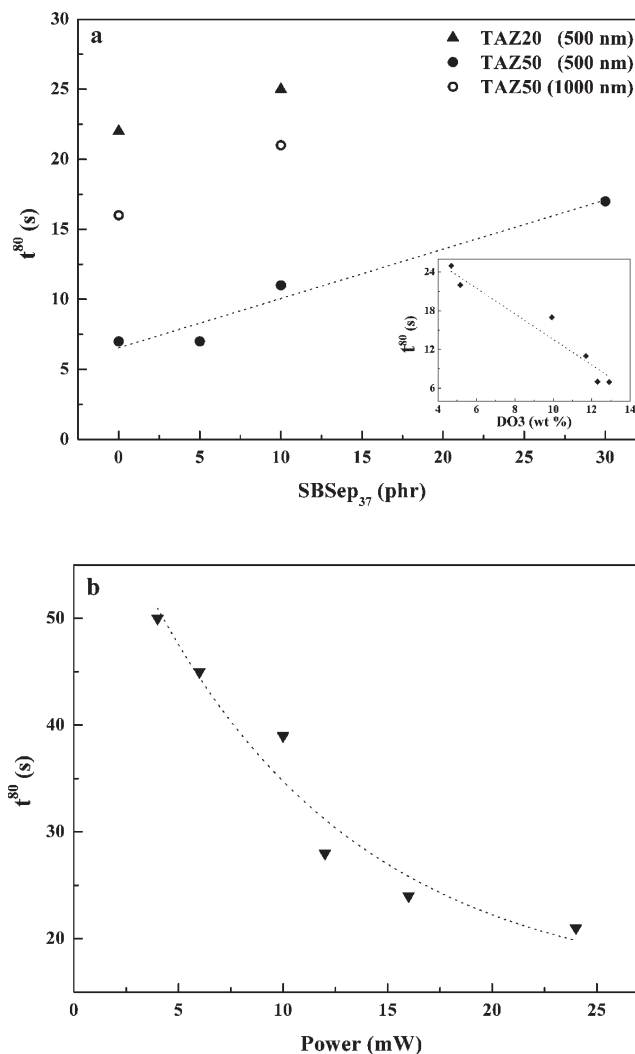


Figure 6. Time necessary to achieve 80% of maximum birefringence as a function of (a) SBSep₃₇ content and film thickness (in the inner graph, the dependence on azobenzene ratio is plotted) and (b) power of the writing beam.

at point C, in order to remove the remaining birefringence, circularly polarized light was introduced, which completely eliminated the dipole orientation. This mode of writing effectively returned the films to the isotropic state, thereby erasing the previously encoded information.

In general, the main difference in curves of Figure 5 is that the induced birefringence clearly increased by the increase of TAZ content. However, a higher rate of birefringence growth as well as a higher remaining birefringence can also be noticed with increasing TAZ content. In what follows, the influence of these parameters will also be addressed.

Focusing on the rate of birefringence growth, the time interval necessary to achieve 80% of saturated birefringence level, t^{80} , is plotted in Figure 6. In particular, Figure 6a shows the influence of azobenzene concentration, SBSep₃₇ content and film thickness in the time necessary to photoinduced anisotropy when films were irradiated with 6 mW of beam power. As it is shown, t^{80} was clearly reduced when increasing the azobenzene content in the samples. This behavior can be explained in terms of a thermal effect. That is to say, an increase in the writing beam absorption

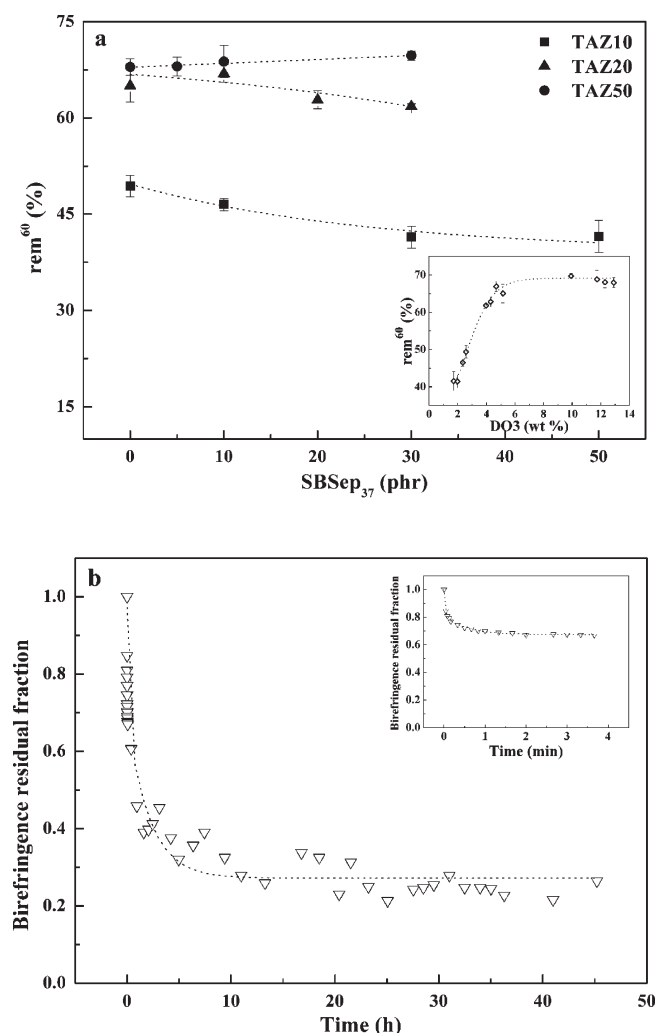


Figure 7. (a) Remaining birefringence after 60 s of turning off the writing beam as a function of SBSep₃₇ and TAZ content (in the inner graph is plotted the dependence on azobenzene ratio). (b) Residual fraction of birefringence after 45 h of turning off the writing beam for a film of TAZ50-SBSep₄₆S (in the inner graph is plotted a magnification of the curve during first 4 min).

occurred upon increasing the azo-chromophore concentration, which could induce sample heating.³⁸ This heating allowed a higher molecular mobility and resulted in a faster writing process. Moreover, t^{80} increased when increasing the amount of SBSep₃₇ in the samples. The increase in SBSep₃₇ content implied a decrease of global DO3 ratio and T_g value. The glass transition temperature can be useful as an approach to predict the freedom of movement of azobenzene units in the epoxy network. The lower the T_g value, the higher the molecular mobility. On the basis of this assumption, t^{80} should decrease as increasing SBSep₃₇ content. But the dependence of azobenzene concentration has also to be considered. By increasing the azo-dye content in the samples, t^{80} decreased even though T_g values were higher. Thus, one can conclude that the thermal effect due to the optical absorption of azobenzene moieties in the wavelength region of the recording light had higher influence on the rate of birefringence growth than the glass transition temperature over the range of values studied. Additionally, in order to analyze the effect of film thickness on the writing rate, t^{80} of films with 50 wt % TAZ

Table 3. Remaining Birefringence of Thermosets Containing 30 phr SBSep₃₇ and Different Amounts of TAZ (10, 20, and 50 wt %)

sample code	DO3 (wt %)	T_g (°C)	rem^{60} (%)
TAZ10-SBSep ₃₇ 30	1.98	121	41.4 ± 1.7
TAZ20-SBSep ₃₇ 30	3.97	122	61.8 ± 0.4
TAZ50-SBSep ₃₇ 30	9.92	121	69.7 ± 0.7

and the same SBSep₃₇ content (0 and 10 phr) but different thickness (500 ± 30 nm or 1000 ± 10 nm) were compared. A slow down of the writing rate was noticed upon increasing the samples thickness. This result may be connected to the fact that as the film thickness increased, the intensity of the writing beam considerably decreased as it propagated throughout the sample, due to large laser intensity absorption of the azobenzene moieties. As a result, the rate of birefringence growth decreased, which is in good agreement with the work reported by Rochon et al.³⁰ devoted to the study of film thickness effect on net phase retardation and writing speed in azo-polymers.

Concerning the influence of the writing intensity on t^{80} , as depicted in Figure 6b, the writing rate grew with the increase in laser beam power. As reported by Natansohn et al.,³⁹ the writing times are controlled by the photon flux, confirming the statistical nature of the process. That is to say, the writing rate was dependent on the number of photons involved in the writing process. The more photons the sample absorbed, the more possible azo-chromophores orientations and the lower t^{80} .

In general, relaxation processes are easier to be studied than orientation ones since effects of heating and isomerization rates are small when the writing beam is turned off. Parameters that have a clear influence on the remaining birefringence are glass transition temperature and cooperative effects that may cause relaxation times to be longer with the increase in azo-chromophore content.²⁹ Figure 7a shows the percentage of remaining birefringence after 60 s of turning off the writing beam (rem^{60}) at 6 mW as a function of SBSep₃₇ ratio and azobenzene concentration in the epoxy thermosets, regardless of films thickness. At higher azo-chromophore contents, the epoxy systems exhibited higher rem^{60} . Furthermore, as can be seen in Table 3, the remaining birefringence increased with the azobenzene concentration in samples with similar T_g values, suggesting that, for the systems studied, the main factor affecting rem^{60} was the azo-dye content. However, a plateau for DO3 contents above 4 wt % was reached, which could indicate that, for these epoxy thermosets and in the range of values evaluated, rem^{60} depended mainly on cooperative interactions among azobenzene groups up to an azo-dye concentration from which the remaining birefringence kept constant.

Nevertheless, it should be pointed out that T_g values of the thermosets prepared varied from 79 to 155 °C, which should favor a good orientation stability of the photoactive chromophores at room and slightly elevated temperatures. Hence, we also studied the long-term stability of the induced birefringence. The residual fraction of birefringence after 45 h of turning off the writing beam at 6 mW for a film of TAZ50-SBSep₄₆S is plotted in Figure 7b. During the first 4 min of turning off the writing beam, birefringence was relaxed around 30%. Then, after 10 h the residual fraction of birefringence was about 0.3 and, though not shown here, it kept stable during several weeks.

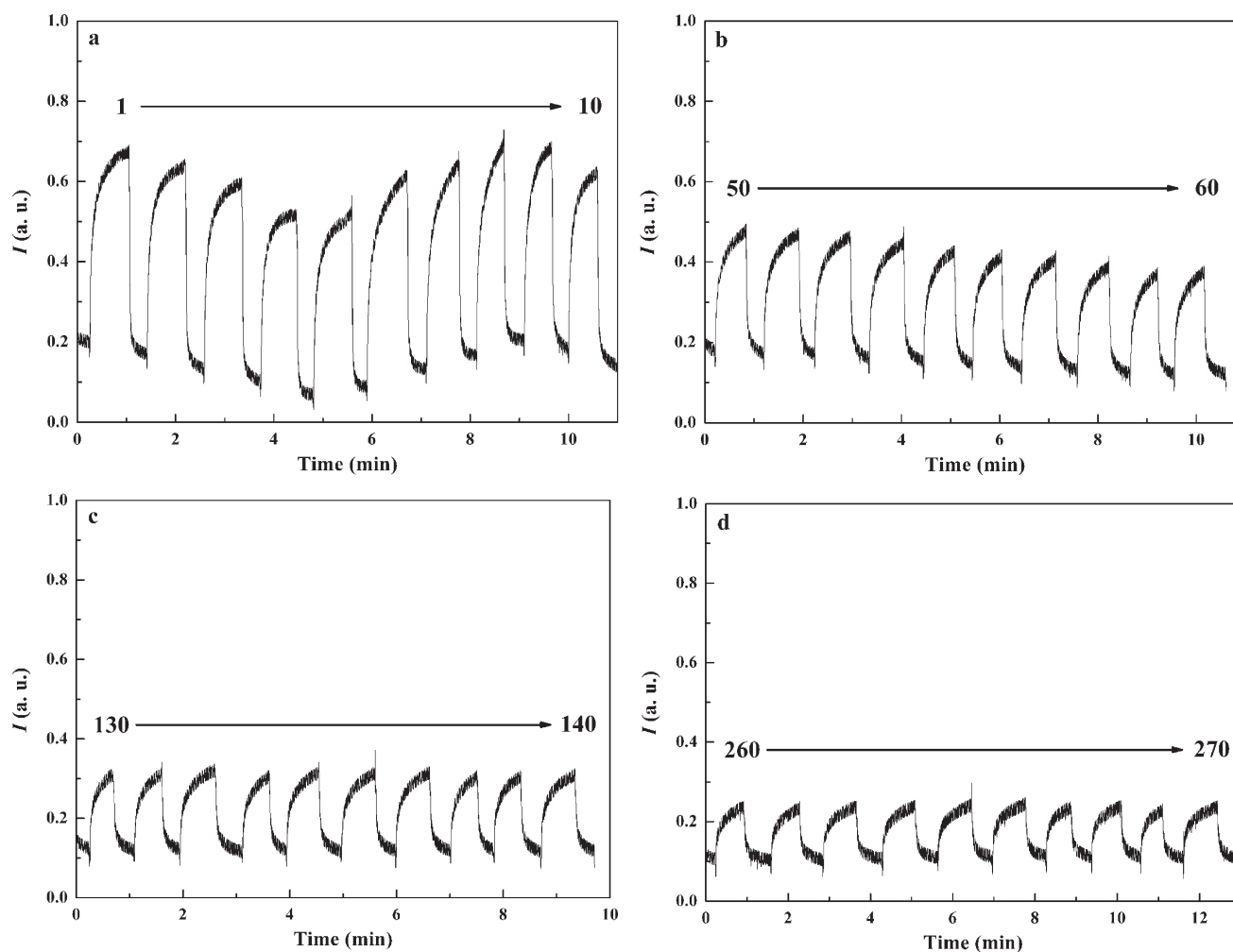


Figure 8. Successive writing-erasing sequences for a film of TAZ20-SBSeP₃₇₁₀: (a) from 1st to 10th cycle, (b) from 50th–60th cycle, (c) from 130th to 140th cycle, and (d) from 260th to 270th cycle. The power of the writing beam is 6 mW.

Our ultimate interest was to study the rewriting stability of the samples. In particular, it was analyzed the maximum transmitted intensity of the reading beam after passing through a film of TAZ20-SBSeP₃₇₁₀ during 270 writing-erasing cycles (Figure 8). During the first 10 cycles up to around 30 cycles, similar transmitted signal was achieved. After 60 writing-erasing sequences in the order of 60% of maximum intensity was still registered and after 140 cycles 50% of maximum intensity was achieved. Finally, after 270 cycles almost 40% of maximum transmitted signal was reached, which means that after 270 cycles there was still a significant birefringence that could be used to distinguish the *on* from the *off* state. Therefore, the ability of this nanostructured epoxy-based thermoset containing azobenzene groups for rewriting was found adequate after consecutive cycles.

CONCLUSIONS

Nanostructured thermosets with different morphologies were obtained from epoxy systems containing azobenzene units using epoxidized SBS as templating agent.

Concerning the morphological study by AFM the main conclusion that can be drawn from this work is that depending on the epoxidation extent and the content of epoxidized SBS and TAZ, nanostructuring of investigated thermosetting systems

took place in different ways. For the lowest epoxidation extent (37 mol %), the formation of nanostructures followed the combined mechanisms of self-assembly of PB chains and reaction-induced microphase separation of PS chains through curing. In addition, self-assembly mechanism was favored when increasing TAZ content in the samples, due to a decrease of miscibility between the epoxy-precursor mixture and the block copolymer before curing. Upon increasing the epoxidation extent to 46 mol %, long-range order nanostructures through RIMS of PS block were achieved for the samples with 10 and 20 wt % TAZ containing 50 and 20 phr BCP, respectively, owing to a higher compatibility of the block copolymer with the epoxy-precursor mixture.

With respect to the analysis of reversible optical storage properties in the developed materials, over the range of values evaluated for the used chromophore and polymer matrix, the azo-dye content was the main factor influencing the optical properties. For very low azobenzene contents (<4 wt %), the poor interaction among photoactive units led to a decrease of Δn_N and remaining birefringence values. However, from around 4 wt % of azo-dye the remaining birefringence and Δn_N kept almost constant in both parent thermosets and the ones modified with epoxidized SBS. Hence, nanostructuring did not have a significant effect on birefringence, because in all studied systems

the azo-chromophores were covalently linked to the epoxy-rich phase, and therefore interactions among azobenzene moieties were similar in parent and nanostructured thermosets. Nonetheless, nanostructuring did not provoke a decay of birefringent properties either and these systems nanostructured by BCP addition could also be used as templates to develop multifunctional materials, for instance by selective dispersion of nanoparticles, thus giving rise to advanced hybrid nanostructured thermosets with interesting combined properties.

AUTHOR INFORMATION

Corresponding Author

*Telephone: +34 943 017 177. Fax: +34 943 017 130. E-mail: inaki.mondragon@ehu.es.

ACKNOWLEDGMENT

Financial support from the EU (Carbon nanotube confinement strategies to develop novel polymer matrix composites, POCO, FP7-NMP-2007, CP-IP 213939-1), Basque Country Government in the frame of Grupos Consolidados (IT-365-07), inanoGUNE (IE09-243), NANOTES (S-PE10UN40) and from the Spanish Ministry of Education and Science (MAT2009-12832) is gratefully acknowledged. The authors also thank the technical and human support provided by SGiker (Macrobehaviour-Mesostructure-Nanotechnology unit). R.F. acknowledges the University of the Basque Country for the grant "Ayuda para la Especialización de Doctores en la UPV/EHU".

REFERENCES

- (1) Paquet, C.; Kumacheva, E. *Mater. Today* **2008**, *11*, 48–56.
- (2) Jiang, H.-J.; Gao, Z.-Q.; Liu, F.; Ling, Q.-D.; Wei, W.; Huang, W. *Polymer* **2008**, *49*, 4369–4377.
- (3) Hanemann, T.; Szabó, D. V. *Materials* **2010**, *3*, 3468–3517.
- (4) Hu, L.; Wu, H.; Du, L.; Ge, H.; Chen, X.; Dai, N. *Nanotechnology* **2011**, *22*, 125202.
- (5) Dierking, I. *Polym. Chem.* **2010**, *1*, 1153–1159.
- (6) Pucci, A.; Bizzarri, R.; Ruggeri, G. *Soft Matter* **2011**, *7*, 3689–3700.
- (7) Kumar, G. S.; Neckers, D. C. *Chem. Rev.* **1989**, *89*, 1915–1925.
- (8) Viswanathan, N. K.; Kim, D. Y.; Bian, S.; Williams, J.; Liu, W.; Li, L.; Samuelson, L.; Kumar, J.; Tripathy, S. K. *J. Mater. Chem.* **1999**, *9*, 1941–1955.
- (9) Delaire, J. A.; Nakatani, K. *Chem. Rev.* **2000**, *100*, 1817–1846.
- (10) Natansohn, A.; Rochon, P. *Chem. Rev.* **2002**, *102*, 4139–4175.
- (11) Yesodha, S. K.; Sadashiva Pillai, C. K.; Tsutsumi, N. *Prog. Polym. Sci.* **2004**, *29*, 45–74.
- (12) Oliveira, O. N., Jr.; Dos Santos, D. S., Jr.; Balogh, D. T.; Zucolotto, V.; Mendonça, C. R. *Adv. Colloid Interface Sci.* **2005**, *116*, 179–192.
- (13) Zhao, Y.; Ikeda, T. *Smart light-responsive materials: azobenzene-containing polymers and liquid crystals*; John Wiley & Sons: Hoboken, NJ, 2009.
- (14) Fdez. de Negraro, F.; Llano-Ponte, R.; Mondragon, I. *Polymer* **1996**, *37*, 1589–1600.
- (15) Ramos, J. A.; Blanco, M.; Zalakain, I.; Mondragon, I. *J. Colloid Interface Sci.* **2009**, *336*, 431–437.
- (16) Leonardi, A. B.; Fasce, L. A.; Zucchi, I. A.; Hoppe, C. E.; Soulé, E. R.; Pérez, C. J.; Williams, R. J. *Eur. Polym. J.* **2011**, *47*, 362–369.
- (17) Kosonen, H.; Ruokolainen, J.; Nyholm, P.; Ikkala, O. *Polymer* **2001**, *42*, 9481–9486.
- (18) Leibler, L. *Prog. Polym. Sci.* **2005**, *30*, 898–914.
- (19) Jaffrennou, B.; Portal, J.; Méchin, F.; Pascault, J. P. *Eur. Polym. J.* **2008**, *44*, 3439–3455.
- (20) Ritzenthaler, S.; Court, F.; David, L.; Girard-Reydet, E.; Leibler, L.; Pascault, J. P. *Macromolecules* **2002**, *35*, 6245–6254.
- (21) Dean, J. M.; Grubbs, R. B.; Saad, W.; Cook, R. F.; Bates, F. S. *J. Polym. Sci., Part B: Polym. Phys.* **2003**, *41*, 2444–2456.
- (22) Hermel-Davidock, T. J.; Tang, H. S.; Murray, D. J.; Hahn, S. F. *J. Polym. Sci., Part B: Polym. Phys.* **2007**, *45*, 3338–3348.
- (23) Fan, W.; Wang, L.; Zheng, S. *Macromolecules* **2010**, *43*, 10600–10611.
- (24) Serrano, E.; Larrañaga, M.; Remiro, P. M.; Mondragon, I.; Carrasco, P. M.; Pomposo, J. A.; Mecerreyes, D. *Macromol. Chem. Phys.* **2004**, *205*, 987–996.
- (25) Ocano, C.; Tercjak, A.; Martín, M. D.; Ramos, J. A.; Campo, M.; Mondragon, I. *Macromolecules* **2009**, *42*, 6215–6224.
- (26) Gutiérrez, J.; Tercjak, A.; Mondragon, I. *J. Phys. Chem. C* **2010**, *114*, 22424–22430.
- (27) Fernández, R.; Mondragon, I.; Oyanguren, P. A.; Galante, M. J. *React. Funct. Polym.* **2008**, *68*, 70–76.
- (28) Ocano, C.; Tercjak, A.; Serrano, E.; Ramos, J. A.; Corona-Galván, S.; Parellada, M. D.; Fernández-Berridi, M. J.; Mondragon, I. *Polym. Int.* **2008**, *57*, 1333–1342.
- (29) Mendonça, C. R.; dos Santos, D. S., Jr.; Balogh, D. T.; Dhanabalan, A.; Giacometti, J. A.; Zilio, S. C.; Oliveira, O. N., Jr. *Polymer* **2001**, *42*, 6539–6544.
- (30) Rochon, P.; Bissonnette, D.; Natansohn, A.; Xie, S. *Appl. Opt.* **1993**, *32*, 7211–7280.
- (31) Song, O. K.; Wang, C. H.; Pauley, M. A. *Macromolecules* **1997**, *30*, 6913–6919.
- (32) Takase, H.; Natansohn, A.; Rochon, P. *J. Polym. Sci., Part B: Polym. Phys.* **2001**, *39*, 1686–1696.
- (33) Sekkat, Z.; Yasumatsu, D.; Kawata, S. *J. Phys. Chem. B* **2002**, *106*, 12407–12417.
- (34) Rodríguez, F. J.; Sánchez, C.; Villacampa, B.; Alcalá, R.; Cases, R.; Millaruelo, M.; Oriol, L. *Polymer* **2004**, *45*, 2341–2348.
- (35) Fernández, R.; Mondragon, I.; Galante, M.; Oyanguren, P. *J. Polym. Sci., Part B: Polym. Phys.* **2009**, *47*, 1004–1014.
- (36) Gimeno, S.; Forcén, P.; Oriol, L.; Piñol, M.; Sánchez, C.; Rodríguez, F. J.; Alcalá, R.; Jankova, K.; Hvilsted, S. *Eur. Polym. J.* **2009**, *45*, 262–271.
- (37) Sáiz, L. M.; Orofino, A. B.; Ruzzo, M. M.; Arenas, G. F.; Oyanguren, P. A.; Galante, M. J. *Polym. Int.* **2011**, *60*, 1053–1059.
- (38) Dhanabalan, A.; Mendonça, C. R.; Balogh, D. T.; Misoguti, L.; Constantino, C. J. L.; Giacometti, J. A.; Zilio, S. C.; Oliveira, O. N., Jr. *Macromolecules* **1999**, *32*, 5277–5284.
- (39) Natansohn, A.; Rochon, P.; Gosselin, J.; Xie, S. *Macromolecules* **1992**, *25*, 2268–2273.